Published in final edited form as:
Appl Opt. 2010 August 10; 49(23): 4343–4354. doi:10.1364/AO.49.004343.

Multi-projection fluorescence optical tomography using a hand-held probe-based optical imager: Phantom studies

Jiajia Ge, **Sarah J Erickson**, and **Anuradha Godavarty***
10555 W. Flagler, St., EC 2675, Optical Imaging Laboratory, Dept of Biomedical Engineering, Florida International University, Miami, FL, 33174

Jiajia Ge: gejiajia@gmail.com; Sarah J Erickson: sarah.erickson@fiu.edu; Anuradha Godavarty: godavart@fiu.edu

Abstract

A hand-held probe based optical optical imager has recently been developed towards three-dimensional tomography. In this study, the improvement of target depth recovery was demonstrated using a multi-projection technique on large slab phantoms using 0.45 cc fluorescing target(s) (with 1:0 contrast ratio) of 1.5 to 2.5 cm deep. Tomographic results using single- and multi (here dual) projection measurements (with and without *a priori* information of target location) were compared. In all experimental cases, the use of multi-projection measurements along with *a priori* information recovered target depth and location closer to its true values, demonstrating its applicability for clinical translation.

Keywords

Optical Imaging; Hand-held probe; Fluorescence; Frequency-Domain; Image Reconstructions; Multi-projection; Intensified CCD camera

1. Introduction

Ongoing efforts in optical imaging and tomography are focused on the clinical translation of the technology towards early-stage breast cancer diagnostics and other varied functional imaging applications. In the process, hand-held optical imagers are rapidly emerging as an alternate to the bulky optical imagers due to their portability and flexibility to image any tissue volume and geometry with a cost-effective instrumentation set-up [1–13]. However, the currently available hand-held based optical imagers have not been developed to perform three-dimensional (3-D) tomographic imaging without guidance from other imaging modalities. Recently, a novel hand-held probe based optical imager has been developed in our Optical Imaging Laboratory (OIL) towards 3-D tomographic imaging on large tissue volumes [14–15]. Preliminary 3-D tomographic imaging was successfully demonstrated using frequency-domain fluorescence measurements obtained from large slab phantoms (~ 650 ml volume) employing the hand-held probe based imager. These fluorescence reflectance measurements were acquired from a single location on a phantom face that was closer to the target (i.e. using a single projected image of the phantom). Although 3-D target location and volume were tomographically reconstructed, the recovered target depth was always closer to the imaging plane in comparison to the true depth. Similar observations of limited target depth recovery were made by other researchers using optical imaging systems that provided only reflectance measurements (similar to our hand-held optical imager). Improvement in target depth recovery

*Corresponding author: godavart@fiu.edu.

is possible by acquiring trans-illumination measurements apart from reflectance measurements. However, a hand-held probe based imager is typically limited to obtaining reflectance measurements; although reflectance measurements can be obtained at multiple locations or angles on the tissue geometry towards improved tomographic resolution.

Multi-projection and dual-projection technique for diffusive optical tomography (DOT) has been performed on slab geometry by Markel *et al* [16–17]. Their simulated slab phantom studies demonstrated that multiple projections can significantly improve the spatial resolution during tomography. Similar observations were made by Lasser *et al* [18] and Deliolanis *et al* [19] during their small animal fluorescence tomography studies. In their study, when the number of projections around a 360°-cylinder enclosing a ratincreased up to 18 projections with respect to single or fewer number of projections, the spatial resolution of the tomographically reconstructed target (or tumor) significantly enhanced. However, both the above studies focused on spatial resolution instead of target depth recovery, which has not been an issue for their imaging systems since it acquired trans-illumination (or transmittance) measurements.

In the current work, a multi-projection based imaging technique will be employed towards fluorescence-enhanced optical tomography studies on large phantoms (~ 650 ml) using a hand-held probe based optical imager that acquires only reflectance measurements using simultaneous illumination based measurement geometry (over the widely used sequential illumination based geometry). This work is different from our past work using the hand-held optical imager, wherein only single project based imaging was performed towards 3D tomography studies (thus limited the target depth recovery).

Additionally, unlike the past work by other researchers [16–17], where multi-projection technique acquired reflectance and trans-illumination measurements (with multi-source projections onto fixed detector rings), the multi-projection technique in this case will involve the rotation of the hand-held probe (containing both sources and detectors) onto multiple faces of the tissue phantom. Although the current approach allows the acquisition of only reflectance measurements, the flexibility to image using a hand-held probe onto any tissue volume and curvature make the imager advantages in a clinical setting. The effect of using only reflectance measurements from multiple projections (or scans) towards improvement in the reconstructed target depth will be assessed with respect to tomographic imaging employing reflectance measurements from a single-projection (or scan). The details of the hand-held probe based optical imager and the frequency-domain fluorescence-based experimental studies performed on large volume phantoms (~ 650 ml) are described in the following sections. Further, 3-D reconstruction results from single and multi-projection measurements are compared. In addition, *a priori* information of the possible target location obtained from multiple projections of 2-D surface images are used in order to determine their impact on the reconstruction quality.

2. Material and Methods

2.1. Instrumentation

A hand-held probe based optical imager is used for performing fluorescence-enhanced optical imaging studies on slab phantoms. The imaging system includes a hand-held probe, a laser diode based light source, and a gain modulated intensified charge-coupled device (ICCD) based detection system (see Fig. 1) [15]. The hand-held probe consists of a probe head of 5×10 cm^2, a custom-built collection fiber bundle and a source fiber bundle [14]. Six simultaneous illumination fibers and 165 collection fibers are arranged on the probe head as shown in Fig. 1(b). The intensity of 6 simultaneous point sources on the probe head are measured using an optical power meter (PM 100, Thorlabs Inc., Newton, NJ) and are accounted into tomography studies. The principle behind this frequency-domain ICCD based optical imager is as described

below. Initially, the modulated laser light from the laser diode (530 mW, HPD1005-9MM, Intense Ltd., North Brunswick, NJ) illuminates the tissue phantom surface via simultaneous illuminating fiber(s) of the hand-held probe. The NIR signal emitted from the tissue phantom surface is acquired by collection fibers of the hand-held probe and imaged using a16-bit, 1024×1024 pixel CCD camera (PI-SCX 7495-0002, Roper Scientific, Trenton, NJ) that is optically coupled with an image intensifier (FS9910, ITT Night Vision, VA). A focusing lens (50mm, f/1.8D AF model, Nikon Inc., Melville, NY) for image focus, and interference filters (HRF-830.0, blocking OD 6 & F-830.0, blocking OD 4, CVI Laser, Albuquerque, NM) for excitation light rejection are coupled to the ICCD camera via a lens assembly. The imaging system is operated in the homodyne mode, meaning that both the source and detector ends are modulated at the same frequency (here 100 MHz). The two frequency synthesizers generating the radio frequency (RF) signal at the source end (HP 8656B, Hayward, CA) and detector end (PTS 310, Programmed Test Sources Inc., Littleton, MA) are phase locked. By introducing phase delays varying from 0 to 2π (here 32 delays) between the two frequency synthesizers, steady-state phase-sensitive intensity images are acquired [15,20]. Fast Fourier Transforms (FFT) is used to extract the amplitude and phase shift information from the acquired steady-state images. The extracted amplitude and phase shift data are then used towards tomography studies. For all experimental cases, a subtraction-based postprocessing technique was employed for eliminating excitation leakage. By subtracting the background noise (i.e. measurements obtained from homogeneous non-fluorescing phantoms) from fluorescence optical measurements obtained from a given experimental case, the excitation leakage can be partially removed. More details of the instrumentation and the data acquisition procedure can be found elsewhere [15].

2.2. Phantom studies

A transparent acrylic container filled with 1% Liposyn solution (volume of 10×6.5×10 cm^3) was used as tissue phantom (see Fig. 1(c)). A hollow clear plastic sphere (volume of 0.45cm^3) filled with 1μM Indocyanine Green (ICG) in 1% Liposyn solution was used to mimic a single target (or tumor). Sodium polyaspartate (MW 3000–8000) (Sigma-Aldrich Chemical Co., St. Louis, CO) was used as a stabilizer for ICG. The optical properties of 1% Liposyn solution at both 785nm and 830nm were measured using a single-pixel frequency domain homodyne system (custom-built in OIL). The optical properties of the fluorescence target were calculated from the contrast agent's concentration and extinction coefficient (listed in Table 1) [20].

Phantom studies were performed at different target locations and depths (1.5, 2 and 2.5cm) as shown in Table 2. Frequency-domain reflectance measurements of the fluorescence signal were acquired on all sides of the slab phantom (Sides A, B, C and D) as shown in Fig. 1(c). Since the phantom size is large (10×6.5×10 cm^3), detection of the target is not feasible from all sides of the phantom, as light tends to exponentially decay when it propagates through the tissue-mimicking medium. Hence, in all our experimental cases, the target positioning was chosen such that it can be detected from at least two sides of the phantom, in order to assess the impact of multi-projection imaging on 3-D tomography. The tomographic target depth recovery using only reflectance-based optical measurements (from single-projection) tend to degrade beyond 1.5 cm as observed by other researchers as well [15,21–25]. Hence our studies were not focused on depths smaller than 1.5 cm, but begin from 1.5 cm and go further deep. The target location (centroid) during various experimental cases is listed in Table 2 and its depth with respect to different sides of the phantom (i.e. Sides A, B, C, and D) is also provided. During surface imaging, the target was not detectable when imaged from sides C and D due to the greater target depths with respect to those sides (see Table 2). Hence, only measurements taken from Sides A and B of the phantom were employed into 2-D studies because the post-subtraction signal intensity detected from Sides C and D is only at noise level.

2.3. Multi-projection based fluorescence surface imaging

Frequency-domain fluorescence measurements (i.e. amplitude and phase-shift) were obtained for the different experimental cases. The detected amplitude at each imaging plane (i.e. Sides A and B) are shown as 2-D surface contour plots using Tecplot 10 (Tecplot, Inc., Bellevue, Washington). The 2-D location of the data point that has maximum amplitude on the surface contour plot was estimated as center of the target. By projecting the target information obtained from each 2-D imaging plane onto a simulated 3-D phantom, a rough estimate of the 3-D target location was obtained.

2.4. Three-dimensional image reconstructions

Three-dimensional image reconstructions were performed using a computationally efficient approximate extended Kalman filter (AEKF) algorithm [15,20,26], in order to obtain the 3-D map of the fluorescence absorption coefficient at excitation wavelength (μ_{axf}) over the entire phantom volume by solving the coupled diffusion equations using a Galerkin-based finite element approach. The AEKF algorithm recursively updated the unknown parameter (μ_{axf}) and parameter error covariance (i.e. the spatially variant error between measurements from each iteration) until the latter was less than the convergence criteria (described below). The inverse process was damped and regularized by measurement error covariance (i.e. the spatially variant error between each repeated experimental measurements), and the model error covariance (i.e. the spatially variant error between experimental and simulated measurements), which was empirically assigned as of measurement error covariance [15,26]. As an initial guess, the unknown parameter (μ_{axf}) was assumed to be homogeneous with an arbitrary small value of 0.003 cm^{-1} for the entire phantom, and the parameter error covariance was arbitrarily set to 0.01. The reconstructions were considered converged when the root mean square output error (RMSE) <0.005 or iteration number was equal to 50 (whichever criteria was first met). In all these studies, the reconstructed fluorescence absorption (μ_{axf}) distribution is presented as 3-D iso-surface plots, which applied a cut-off value that was chosen based on the first break point of μ_{axf} histogram plot to differentiate target region from background. The same cut-off value was also applied to quantitative comparison between recovered and true target details in terms of 3-D target location (i.e. the centroid of the 3-D target) [15].

The 3-D tomography studies performed in the current work can be categorized into three studies: i) Study I: Single-projection based tomography; ii) Study II: Multi-projection based tomography without *a priori* information; and iii) Study III: Multi-projection based tomography with *a priori* information. The details of these different tomography studies are listed in Table 3.

The finite element mesh generated using Gambit software (ANSYS Inc., Lebanon, NH) employed tetrahedral elements that were finely discretized with surface triangular elements spaced 0.25 cm apart, only on the imaging surfaces (i.e. Sides A or B for Study I, and both Sides A and B for Study II and III), and all the tetrahedral elements between 0.25 and 0.5 cm apart. Upon discretizing two surfaces of the cubical phantom with finer elements (for Study II and III) over only one surface (for Study I), the total number of nodes (in other words, the unknown parameters) increased from 10835 to 18860, respectively, causing computational memory limitations. Hence, a coarser mesh of total node number of 8008 was generated for Study II and Study III, with the 0.5 cm spaced triangular elements on the imaging surfaces (Sides A and B), and all the tetrahedral elements spaced 0.5 cm as well.

2.4.1. Study I: Single-projection based tomography—The single-projection based tomography was performed in order to determine if the additional measurements from multi-projection imaging aid in target depth recovery during tomography studies (i.e. Study II and III). In this study, the measurements from Sides A and B were used independently as single-

projection based measurements towards 3-D tomographic reconstructions. No *a priori* information was applied towards the initial μ_{axf} distribution.

2.4.2. Study II: Multi-projection based tomography without a priori information—The dual-projection measurements from Sides A and B (and not measurements from all four sides, due to reasons described in Section 2.2) were incorporated towards tomographic reconstructions in Study II. No *a priori* information was applied towards the initial μ_{axf} distribution.

2.4.3. Study III: Multi-projection based tomography with a priori information—Study III is also a dual-projection based reconstruction study (as in Study II), but with *a priori* information applied towards initial μ_{axf} distribution. The *a priori* information is the possible target location estimated from 2-D surface fluorescence images of the phantom (Sides A and B). By performing simple back-projection based on two perpendicular 2-D surface images, a rough estimation of possible target location is obtained and incorporated into tomography as a volumetric region with elevated initial μ_{axf} value. This *a priori* volumetric region is estimated using different cut-off values such as 90%, 80% and 60% of maximum amplitude on the surface images. The 90% cut-off value tends to generate very small, even zero *a priori* volume, hence its results were not included in Study III. The elevated μ_{axf} value was arbitrarily chosen as 20 and 10 times higher than the initially assumed background μ_{axf} value (0.003 cm^{-1}), i.e. 20:1 and 10:1 respectively. Different cases of elevated μ_{axf} contrast ratios and volumetric regions were chosen in order to determine their effect on the quality of 3-D image reconstructions (as listed in Table 3).

3. Results and Discussion

3.1. Multi-projection based fluorescence surface imaging

Frequency-domain optical measurements were obtained from all four sides of the phantom in each experimental case, but only measurements from Sides A and B contained fluorescence signals above the noise floor in all the cases (see Section 2.2). The combined surface images obtained from Sides A and B are shown in Fig. 2 for all the experimental cases, and 3-D target location estimated from these surface images were listed in Table 4.

For example, the 2-D surface plot of case # 3 (Side A of Fig. 2(c)) showed that the target location was estimated at [x,y] = [2.4, 3.1] cm (always taken at the point of maximum fluorescence amplitude on the contour plot) at X-Y plane. From the surface plot at Z-Y plane (Side A of Fig. 2(c)), which showed the detected amplitude distribution on Side B of the phantom, the target location was estimated at [z,y] = [1.7, 2.6] cm. By combining the estimated 2-D target locations obtained from both sides, the target can be localized at [x,y,z] = [2.4, 2.6~3.1, 1.7] cm, which is close to true target location of [x,y,z] = [2.5, 2.5, 2] cm. The comparison between the estimated 3-D target location with respect to true target location for all experimental cases is listed in Table 4. From Fig. 2 and Table 4, it is evident that the target 3-D location can be tentatively estimated using surface measurements obtained from at least two sides (i.e. dual-projection) of the phantom.

It can also be observed that the estimated 3-D target locations are slightly distance-off from the true target locations (listed in Table 4) for all experimental cases. This distance-off is possibly due to the uncertainty in placing the phantom/target in the dark room, or the limited number of detection points on the probe (0.5cm apart). The latter can be overcome by moving probe along the tissue surface with a small step size (i.e. 0.1 to 0.2cm) in the future studies.

Surface contour plots represent a diffuse area of fluorescence signal distribution and are not capable of estimating (or quantifying) the target size and/or its optical properties. In order to

perform quantitative breast imaging in terms of 3-D target localization and characterization (i.e. optical properties), 3-D tomography studies are essential and hence performed in the current work using multi-projection measurements.

3.2. Multi- projection fluorescence optical tomography

Three-dimensional tomography studies were performed on a $10\times6.5\times10cm^3$ slab phantom employing the multi-projection measurements. Only measurements from two projections (Sides A and B) were incorporated into 3-D reconstructions (see Section. 2.4.2), and the results are described for each experimental case using single- or multi-projection measurements (with or without *a priori* information) as described in Table 3.

3.2.1. Study I: Single-projection based fluorescence tomography—The reconstruction results based on single-projection (i.e. using measurements from only one side of the phantom, here Side A or B) are listed in Tables 5 to 9 for experimental cases 1 to 5, respectively, and also shown as 3-D iso-surface contour plots in Fig. 3. From Fig. 3(a) to 3(e) (tomography results using Side A measurements) and 3(f) to 3(g) (tomography results using Side B measurements), it can be observed that the reconstructed target location agreed with its true location in transverse direction (parallel to the imaging plane). However the target depth, which was perpendicular to the imaging plane (i.e. z axis for Side A measurement, x axis for Side B measurements), reconstructed closer to the phantom surface in all the experimental cases 1 to 5. The limitation in depth recovery using single-projection measurements could possibly be due to the physics of using only reflectance measurements towards tomographic reconstructions, as also observed by other researchers in the past [15,21–25]. The underestimated target depth with respect to one imaging plane can possibly be recovered using measurements obtained from a different imaging plane (i.e. another projection). For example, in experimental case 1 the target depth of 2cm towards Side A (z-axis) is recovered at 0.5cm when using Side A measurements towards tomography. However this target depth recovery improves to 1.9cm when using Side B measurements during tomography, since z-axis in this case is the transverse direction with respect to the imaging plane and not the depth. This suggested a possibility in target depth recovery improvement, by incorporating multi-projection (here at least dual) measurements towards 3-D tomographic reconstructions.

3.2.2. Study II: Multi-projection tomography without a priori information—The reconstruction results based on multi-projection measurements (i.e. using measurements from both sides the phantom, here Sides A and B) without *a priori* information were listed in Tables 5 to 9 for experimental cases 1 to 5, respectively, and also shown as 3-D iso-surface contour plots in Fig. 4. It was observed from Fig. 4 (tomography results using both Sides A and B measurements) that the reconstruction results did not effectively improve the target depth recovery in comparison to using single-projection based measurements. Instead the target tends to be reconstructed as single or two targets that are closer to their reconstructed locations using the two independent single-projection measurements (from Sides A or B or both sides), along with artifacts in some cases. Similar tomography results were obtained upon using simulated measurements instead of experimental data, further emphasizing that the inability to reconstruct a single target closer to the true location may possibly be from the physics of how simultaneously illuminating (here six) light propagates and interacts with a target, or from the inverse algorithm employed.

Although multi-projection based tomography studies (simulated or on small animals) have been performed in the past by other researchers [16–19], no issues of multiple target recovery of a single true target were observed from employing multi-projection measurements. This is possibly because the experimental system in the current study is different in terms of using simultaneously illuminating sources (over the commonly used sequential sources), reflectance

based measurements (over trans-illumination measurements employed in the past multi-projection based measurements). Alternately, differences in the computational tools (or inverse algorithms) employed may also be the reason for the quality of image reconstructions. Future experimental studies using our hand-held optical imager will involve the use of sequential source illumination and alternate reconstruction algorithm(s), in order to determine the possible cause of reconstructing two targets instead of one as observed from most of the current cases.

In short, the current experimental and simulated results indicated that simple incorporation of multi-projection measurements into tomographic reconstructions is not sufficient for improvement in target depth recovery, using our hand-held probe based optical imager. Hence, in our following tomography study, we implemented *a priori* information of the estimated target's 3-D location (and volume) in order to assess its effectiveness in reconstructing a single target with improved depth recovery. The reconstruction results were compared to those obtained from Study I and II.

3.2.3. Study III: Multi-projection tomography with a priori information—*The* reconstruction results based on multi-projection measurements (i.e. both Sides A and B of the phantom) incorporated with different *a priori* target volumetric regions and initial μ_{axf} guesses (as described in Table 3) were listed in Tables 5 to 9 for experimental cases 1 to 5, respectively. Three-dimensional iso-surface contour plots were generated using the reconstruction results for all experimental cases, but only a portion of the results (using *a priori* information obtained using 80% cut-off values and 10:1 optical contrast for experimental cases 1 to 5) are shown in Fig. 5, for brevity. For each experimental case, the reconstruction results were first compared within Study III, which was performed using different *a priori* conditions. The average distances off between true and recovered target 3-D location (based on all experimental cases) are 0.48 cm and 0.53 cm for an initial optical contrast of 20:1 and 10:1, respectively of the *a priori* target regions. Since the difference between the recovered and true target location using either of the two initial optical contrast ratios was not significant (~0.5 mm), a smaller contrast for *a priori* region was chosen in order to control the impact of *a priori* information on reconstructions. When the cutoff value of 80% was applied to obtain *a priori* region, the recovered target was consistently but slightly closer to the true target location in all the experimental cases, than when the cut-off value of 60% was applied. The average distance-off between true and recovered target 3-D location (based on all experimental cases) differed by <1.5 mm between the reconstruction results employing the 80% cut-off *vs.* the 60% cut-off values as *a priori* information (average distance-off for 80% and 60% cut-off was 0.44 cm and 0.58 cm, respectively). Hence, the reconstruction results of two-sided measurement with *a priori* information that was based on 80% cut-off values and 10:1 target to background contrast values were chosen for comparing the single (Study I) and multi-projection based (Study III) tomography, and its reconstruction results were shown as 3-D iso-surface contour plots (Fig. 5).

Comparing the reconstruction results from Study I and Study III (guided by the *a priori* information obtained using 80% cut-off and target/background ratio of 10), it was observed that the target localization was significantly improved using multi- (here dual) projection over single-projection based reconstruction results (Fig. 6). The average distance-off between true and recovered target 3-D location for all experimental cases decreased from 1.54cm (Study I) to 0.49cm (Study III), which predominantly is contributed from the improvement in target depth recovery. There was an ~80% improvement in the target depth recovery from Study III over Study I, by estimating the average distance-off between the true and reconstructed target depths. In all experimental cases, the tomography results from Study III recovered the target depth closer to the true depth, unlike the tomography results from Study I. Study II is not included in these comparison studies between single and multi-projection based tomography, since it was difficult to calculate the recovered target 3-D location or depth due to the presence

of multiple artifacts in most experimental cases. But it is evident that *a priori* information is essential during reconstructions performed using multi-projection reflectance measurements. This could be due to the fact that *a priori* information provided an initial guess of true target region that agreed with both sets of measurement, hence made possible the integration of multi-projection data into the reconstruction process. In addition, to the quantified reconstructed target location (centroid, depth), the recovered target volume and reconstructed parameter (μ_{axf}) were estimated from image reconstructions for the various Study I and III. No obvious improvement was observed in terms of these parameters and hence the details are not shown.

Reconstructions were also carried out using such *a priori* information along with single-projection measurements instead of multi-projection measurements. It was observed that the target localization and the recovered target depth improved upon using *a priori* information, although only single-projection measurements were employed during reconstructions. This emphasizes the significance of incorporating *a priori* information towards improved image reconstruction quality in terms of target depth recovery, although only reflectance based measurements were acquired. However, it is more practical in using *a priori* information with multi-projection measurements over single-projection measurements for a hand-held based device, which typically acquires measurements from multiple locations (i.e. multi-projection measurements) on the tissue surface.

Apart from the experimental studies using single target at various depths was performed to demonstrate the effectiveness of the multi-projection approach, simulation studies have also been performed using multiple targets. Upon applying the same multi-projection imaging approach, the target(s) were tomographically detectable close to their true location (results not shown for conciseness). Currently, experimental studies are carried out using multiple targets at varying depths, volumes and contrast ratios.

4. Conclusions

In this paper we introduced *a priori* information guided multi-projection technique towards improvement of target depth recovery in fluorescence-enhanced optical tomography studies, using a hand-held based optical imager. Four projections were originally performed on all four sides of a cubical phantom of $10\times6.5\times10cm^3$ with one fluorescing target embedded, which has different target depth with respect to the four projection surfaces. Among four projections, two projections in which the target depth is higher than 7cm were not taken into account since the corresponding detected signal was at the noise level. The 2-D surface fluorescence images based on two perpendicular projections were combined to obtain a rough estimate of the target 3-D location. The fluorescence signals detected from multi- (here dual) projections were then utilized for fluorescence enhanced optical tomography studies. Both single and multi-projection based tomography was performed for comparison in terms of depth recovery towards both projection faces. The single-projection tomography showed good transverse resolution, but limited depth resolution for the limitation of reflectance measurement as already reported [15,21–25]. The multi-projection tomography that simultaneously incorporated multiple measurement sets from different projections into reconstructions was performed both with and without *a priori* information. When no *a priori* information was provided during reconstructions, the multi-projection tomography not only showed no improvement on target depth recovery, but also degraded reconstruction quality by introducing artifacts for most experimental cases. Upon providing *a priori* information of the 3-D target volumetric region during reconstructions, the tomography was effectively guided and target depth recovery for all experimental cases was improved. This is the first time that multi-projection technique has been implemented to a hand-held probe based optical imager that employed simultaneous multiple point illumination/collection geometry and reflectance based measurements, towards 3-D tomography This study also successfully demonstrated: i) the feasibility of multi-

projection based 2-D surface fluorescence imaging to provide a rough estimation of target 3-D location, that can be used both as *a priori* information for tomography studies or complementary information towards cancer diagnosis; ii) the feasibility of multi-projection tomography using a hand-held probe based optical imager, which is designed to have flexibility of performing multi-projection or multi-scan imaging; and iii) the possibility of improvement in target depth recovery using only reflectance measurements during tomography.

One big challenge for the clinical translation of *a priori* information guided multi-projection technique is its dependence on 2-D surface fluorescence imaging, which is limited by contrast ratio between tumor and background. The current study is based on the best case scenario (i.e. homogeneous background and target/background contrast ratio of 1:0). However, in an actual human tissue, the background is highly heterogeneous and has varied optical properties throughout the tissue volume. Hence a chicken breast phantom study, which is a closer simulation of heterogeneous human breast tissue, has been performed in our laboratory and the improvement of target depth recovery using *a priori* information guided multi-projection technique was also observed from our initial tomography studies (extensive studies are currently carried out). In addition, the fluorescence distribution in tumor and normal tissue also plays an important role in imaging quality. Hence more extensive experimental studies using both homogeneous and heterogeneous phantom with imperfect uptake optical contrast ratios will be performed to enhance the possibilities towards clinical translation. Parallelly, the effectiveness of using (i) excitation signal towards *apriori* information (especially in imperfect uptake contrast ratio cases); and (ii) sequential multiple point illumination over simultaneous illumination, will be assessed towards high quality image reconstructions with greater accuracies.

In the future, this *a priori* information guided multi-projection technique can be extended to other reflectance measurements-based optical imaging systems, such as an area illumination and collection system [22–23], in order to improve the target depth recovery. But unlike the hand-held probe based imager, the reflectance measurements-based optical imaging systems developed by other researchers may require the subject, device or both to move in order to obtain measurements from the entire tissue volume towards tomographic imaging. This in turn requires a method to track the motion of the subject/device and coregister the measurements onto the tissue volume appropriately. Currently, OIL is developing automated real-time coregistration techniques such that the optical measurements obtained from multiple locations on the tissue are automatically coregistered on the tissue volume, in order facilitate 3-D tomographic imaging [27].

Until now, optical tomography studies have only employed *a priori* information of the possible target(s) location with the aid of other imaging modalities such as ultrasound, x-ray, and MRI [13,28–29], in order to improve the target localization. The current study is the first of its kind, where 2-D surface fluorescence images will be used as *a priori* information in order to self-guide the tomographic imaging and possibly improve the reconstruction quality.

In conclusion, our initial cubical phantom studies demonstrated the feasibility of multi-projection based surface imaging and tomography study using a hand-held probe based optical imager. This technique can provide rough target 3-D location using surface images and improve target depth recovery in tomography studies. With more validation using laboratory phantom studies, such as experiments using different phantom shape, target size and number, target/background contrast ratio, it is expected that in the future this hand-held probe based optical imager can be translated into clinical breast imaging.

Acknowledgments

The current work has been funded by National Institutes of Health grant (R15CA119253).

References

1. Tromberg BJ, Coquoz O, Fishkin JB, Pham T, Anderson ER, Butler J, Cahn M, Cross JD, Venugopalan V, Pham D. Non-invasive measurements of breast tissue optical properties using frequency-domain photon migration. Philos Trans R Soc Lond B Biol Sci 1997;352:661–668. [PubMed: 9232853]
2. Tromberg BJ. Optical scanning and breast cancer. Acad Radiol 2005;12:923–924. [PubMed: 16087089]
3. Pham TH, Coquoz O, Fishkin JB, Anderson E, Tromberg BJ. Broad bandwidth frequency domain instrument for quantitative tissue optical spectroscopy. Rev Sci 2000;71:2500–2513.
4. Shah N, Cerussi A, Eker C, Espinoza J, Butler J, Fishkin J, Hornung R, Tromberg BJ. Noninvasive functional optical spectroscopy of human breast tissue. Proc Natl Acad Sci USA 2001;98:4420–4425. [PubMed: 11287650]
5. Shah N, Cerussi AE, Jakubowski D, Hsiang D, Butler J, Tromberg BJ. Spatial variations in optical and physiological properties of healthy breast tissue. J Biomed Opt 2004;9:534–540. [PubMed: 15189091]
6. Jakubowski DB, Cerussi AE, Bevilacqua F, Shah N, Hsiang D, Bulter J, Tromberg BJ. Monitoring neoadjuvant chemotherapy in breast cancer using quantitative diffuse optical spectroscopy: a case study. J Biomed Opt 2004;9:230–238. [PubMed: 14715078]
7. Chen N, Huang M, Xia H, Piao D. Portable near-infrared diffusive light imager for breast cancer detection. J Biomed Opt 2004;9:504–510. [PubMed: 15189088]
8. Chance B, Nioka S, Zhang J, Conant EF, Hwang E, Briest S, Orel SG, Schnall MD, Czerniecki BJ. Breast cancer detection based on incremental biochemical and physiological properties of breast cancers: A six-year, two-site study. Acad Radiol 2005;12:925–933. [PubMed: 16023383]
9. Chance B, Zhao Z, Wen S, Chen Y. Simple ac circuit for breast cancer detection and object detection. Rev Sci Instr 2006;77:064301.
10. No KS, Chou PH. Mini-FDPM and Heterodyne Mini-FDPM: Handheld Non-Invasive Breast Cancer Detectors Based on Frequency Domain Photon Migration. IEEE Trans Circuits Syst [Circuits and Systems I: Fundamental Theory and Applications] 2005;52:2672–2685.
11. No KS, Xie Q, Kwong R, Cerussi A, Tromberg BJ, Chou P. HBS: a handheld breast cancer detector based on frequency domain photon migration with full heterodyne. Proc IEEE BioCAS. 2006
12. Durduran T, Choe R, Yu G, Zhou C, Tchou JC, Czemiecki BJ, Yodh AG. Diffuse optical measurement of blood flow in breast tumors. Opt Lett 2005;30:2915–2917. [PubMed: 16279468]
13. Zhu Q, Kurtzma SH, Hegde P, Tannenbaum S, Kane M, Huang M, Chen NG, Jagjivan B, Zarfos K. Utilizing optical tomography with ultrasound localization to image heterogeneous hemoglobin distribution in large breast cancers. Neoplasia Mar 2005;7:263–70.
14. Jayachandran B, Ge J, Regalado S, Godavarty A. Design and development of a hand-held optical probe towards fluorescence diagnostic imaging. J Biomed Opt 2007;12:054014. [PubMed: 17994902]
15. Ge J, Zhu B, Regalado S, Godavarty A. Three-dimensional fluorescence-enhanced optical tomography using a hand-held probe based imaging system. Med Phys 2008;35:3354–3363. [PubMed: 18697559]
16. Markel VA, Schotland JC. Dual-projection optical diffusion tomography. Opt Lett 2004;29:2019–21. [PubMed: 15455766]
17. Markel VA, Schotland JC. Multiple projection optical diffusion tomography with plane wave illumination. Phys Med Biol 2005;50:2351–64. [PubMed: 15876672]
18. Lasser T, Ntziachristos V. Optimization of 360 degrees projection fluorescence molecular tomography. Med Image Anal 2007;11:389–99. [PubMed: 17524701]
19. Deliolanis N, Lasser T, Hyde D, Soubret A, Ripoll J, Ntziachristos V. Free-space fluorescence molecular tomography utilizing 360 degrees geometry projections. Opt Lett 2007;32:382–384. [PubMed: 17356660]

20. Godavarty A, Eppstein MJ, Zhang C, Theru S, Thompson AB, Gurfinkel M, Sevick-Muraca EM. Fluorescence-enhanced optical imaging in large tissue volumes using a gain modulated ICCD camera. Phys Med Biol 2003;48:1701–1720. [PubMed: 12870578]
21. Godavarty A, Thompson AB, Roy R, Eppstein MJ, Zhang C, Gurfinkel M, Sevick-Muraca EM. Diagnostic imaging of breast cancer using fluorescence-enhanced optical tomography: phantom studies. J Biomed Opt Special edition on Biomedical Optics and Women's Health 2004;9(3):488–496.
22. Joshi A, Bangerth W, Hwang K, Rasmussen JC, Sevick-Muraca EM. Fully adaptive FEM based fluorescence optical tomography from time-dependent measurements with area illumination and detection. Med Phys 2006;33:1299–1310. [PubMed: 16752565]
23. Joshi A, Bangerth W, Hwang K, Rasmussen JC, Sevick-Muraca EM. Plane-wave fluorescence tomography with adaptive finite elements. Opt Lett 2006;31:193–195. [PubMed: 16441027]
24. Kepshire DS, Davis SC, Dehghani H, Paulsen KD, Pogue BW. Subsurface diffuse optical tomography can localize absorber and fluorescent objects but recovered image sensitivity is nonlinear with depth. Appl Opt 2007;46:1669–1678. [PubMed: 17356609]
25. Kepshire DS, Davis SC, Dehghani H, Paulsen KD, Pogue BW. Challenges in sub-surface fluorescence diffuse optical imaging. Proc SPIE 6434 64340V 2007:1–9.
26. Eppstein MJ, Dougherty DE, Hawrysz DJ, Sevick-Muraca EM. Three dimensional bayesian optical image reconstruction with domain decomposition. IEEE Trans Med Imaging 2001;20:147–163. [PubMed: 11341706]
27. Regalado S, Erickson SJ, Zhu B, Ge J, Godavarty A. Automated real-time coregistered imaging using a hand-held probe-based optical imager. Rev Sci Instrum 2010;81:023702. [PubMed: 20192497]
28. Zhang Q, Brukilacchio TJ, Li A, Stott JJ, Chaves T, Hillman E, Wu T, Chorlton M, Rafferty E, Moore RH, Kopans DB, Boas DA. Coregistered tomographic x-ray and optical breast imaging: initial results. J Biomed Opt 2005;10:024033. [PubMed: 15910106]
29. Lin Y, Gao H, Nalcioglu O, Gulsen G. Fluorescence diffuse optical tomography with functional and anatomical a priori information: feasibility study. Phys Med Biol 2007;52:5569–85. [PubMed: 17804882]

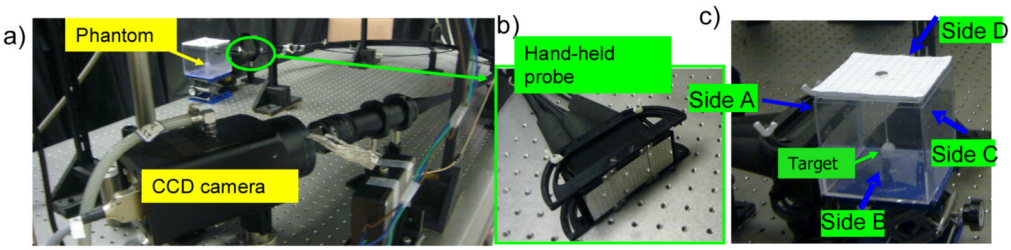

Fig. 1.

The instrumentation of the hand-held probe based ICCD optical imager. a) the entire imaging system; b) the hand-held probe in its flat position; and c) the cubical phantom used for imaging, with the container filled with 1% Liposyn during experiments.

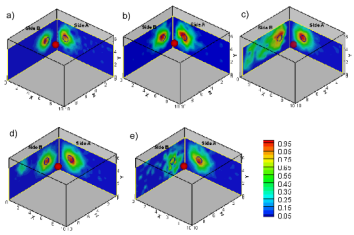

Fig. 2.

The 2-sided surface contour plots of fluorescence amplitude obtained from frequency-domain multi-projection imaging studies for all experimental cases (figure (a) to (e) corresponding to case 1 to 5). The projected 2-D target location is shown as black hollow circles on Sides A and B of the phantom. The solid red sphere in the phantom represents the true 3-D target location. Each surface contour plot was normalized with respect to the maximum amplitude in that particular scan at a given probe location.

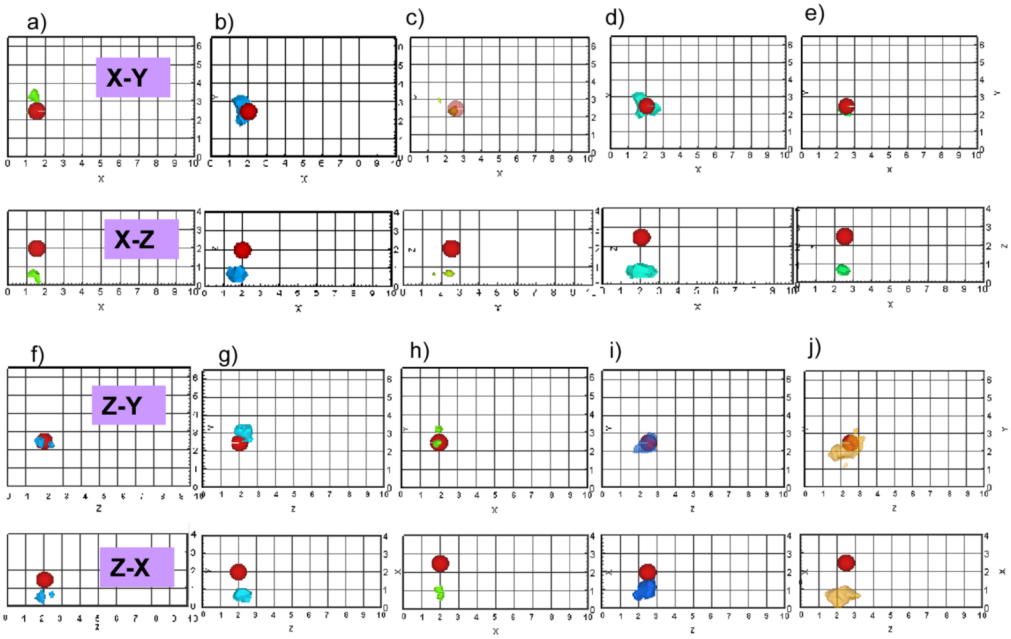

Fig. 3.

Iso-surface contour plots of the 3-D image reconstructions based on single-projection measurements presented in the X-Y and X-Z plane for Side A measurement based reconstructions, Z-Y and Z-X planes for Side B measurement based reconstructions, using 1% Liposyn phantom under perfect uptake conditions for Study I. Tomography studies performed using single-projection based measurements at Side A of phantom (X-Y plane) was shown in (a) to (e) for experimental cases 1 to 5, respectively. Tomography studies performed using single-projection based measurements at Side B of phantom (Z-Y plane) was shown in (f) to (j) for experimental cases 1 to 5, respectively. A single 0.45 cc target was located at [1.5, 2.5, 2] cm in (a) and (f), [2, 2.5, 2] in (b) and (g), [2.5, 2.5, 2] in (c) and (h), [2, 2.5, 2.5] in (d) and (i), and [2.5, 2.5, 2.5] in (e) and (j). The solid sphere in each plot represents the true target location and the irregular solid region represents the reconstructed target location. A cut-off value (selected based on the first break point of histogram plot of μ_{axf}) was applied to iso-surface contour plots in order to differentiate the target from the background. Only 4 cm along the depth is presented in the plot, although the total depth for Side A is Z=10 cm and for Side B is X=10cm.

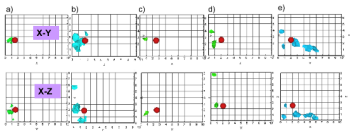

Fig. 4.

Iso-surface contour plots of the 3-D image reconstructions based on measurements from both Side A and Side B of phantom (i.e. X-Y plane and Z-Y plane of phantom) were presented in the X-Y and X-Z planes, using 1% Liposyn phantom under perfect uptake conditions for Study II. A single 0.45 cc target was located at (a) [1.5, 2.5, 2] cm, (b) [2, 2.5, 2] cm, (c) [2.5, 2.5, 2] cm, (d) [2, 2.5, 2.5] cm, and (e) [2.5, 2.5, 2.5] cm. The solid sphere in each plot represents the true target location and the irregular solid region represents the reconstructed target location. A cut-off value (selected based on the first break point of histogram plot of μ_{axf}) was applied to iso-surface contour plots in order to differentiate the target from the background. Only 8 cm along the depth is presented in the plot, although the total depth for Side A is Z=10 cm and for Side B is X=10cm.

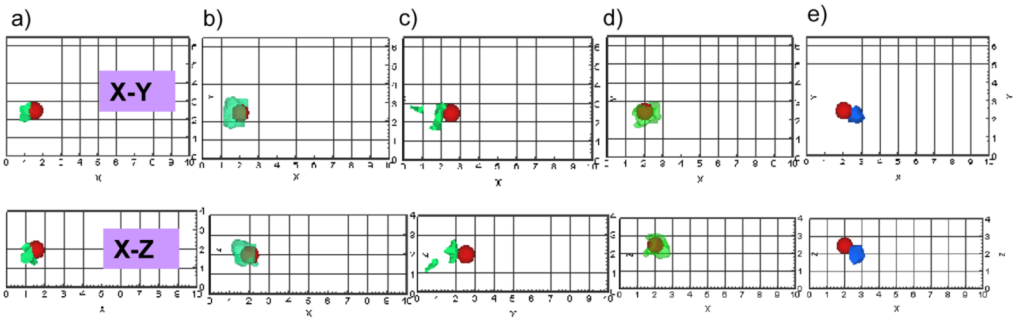

Fig. 5.

Iso-surface contour plots of the 3-D image reconstructions based on measurements from both Side A and Side B of phantom (i.e. X-Y plane and Z-Y plane of phantom) and guided using *a priori* information obtained from 2D surface imaging were presented in the X-Y and X-Z planes, using 1% Liposyn phantom under perfect uptake conditions for Study III. The *a priori* information for each experimental case was obtained using cut-off value of 80% and 10:1 target to background contrast values. A single 0.45 cc target was located at (a) [1.5, 2.5, 2] cm, (b) [2, 2.5, 2] cm, (c) [2.5, 2.5, 2] cm, (d) [2, 2.5, 2.5] cm, and (e) [2.5, 2.5, 2.5] cm. The solid sphere in each plot represents the true target location and the irregular solid region represents the reconstructed target location. A cut-off value (selected based on the first break point of histogram plot of μ_{axf}) was applied to iso-surface contour plots in order to differentiate the target from the background. Only 4 cm along the depth is presented in the plot, although the total depth, Z=10 cm for Side A and X=10cm for Side B of the phantom.

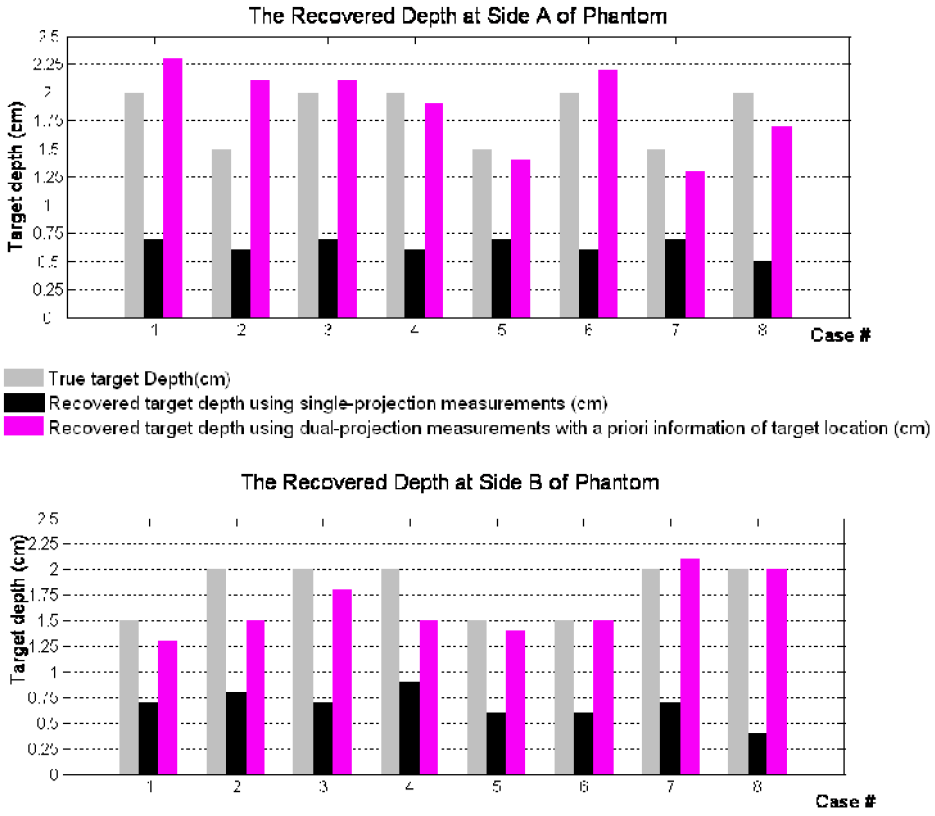

Fig. 6.

The comparison of recovered target depth using single-projection, dual-projection measurements along with a priori information of target location with true target depth. The top figure showed target depth with respect to side A of phantom, while the bottom figure showed target depth with respect to side B of phantom.

Table 1

Optical properties of phantom and fluorescent target for all experimental cases.

Optical Properties	μ_{ax} (cm^{-1})		μ_{am} ($cm\ cm^{-1}$)		μ_{sx}[e] ($cm\ cm^{-1}$)	μ_{sm}[f] ($cm\ cm^{-1}$)	Φ[g]	τ[h] (nsec)
	μ_{axf}[a]	μ_{axi}[b]	μ_{amf}[c]	μ_{ami}[d]				
Target	0.3	0.04	0.506	0.046	10.87	9.82	0.0108	0.56
Background	0.00	0.051	0.00	0.054	9.34	7.42	8	

[a] & [c] Absorption coefficient of the fluorophores at excitation and emission wavelengths, respectively

[b] & [d] Absorption coefficient of the chromophores at excitation and emission wavelengths, respectively

[e] & [f] Scattering coefficient of the chromophores at excitation and emission wavelengths, respectively

[g] & [h] Quantum efficiency and life time of ICG, respectively

Table 2

The target location details for all experimental cases.

		Target depth (cm)			
Case#	**Target Location (cm)**	**w.r.t Side A**	**w.r.t Side B**	**w.r.t Side C**	**w.r.t Side D**
1	[1.5 2.5 2]	2	1.5	8	8.5
2	[2 2.5 2]	2	2	8	8
3	[2.5 2.5 2]	2	2.5	8	7.5
4	[2 2.5 2.5]	2	2.5	8	7.5
5	[2.5 2.5 2.5]	2.5	2.5	7.5	7.5

Table 3

The details of multi-projection based fluorescence-enhanced optical tomography studies

	Input Data	*A priori* Volume	Initial guess of μ_{axf} (cm^{-1})
Study I	Side A measurements	N/A	0.003
	Side B measurements	N/A	0.003
Study II	Side A + Side B measurements	N/A	0.003
Study III	Side A + Side B measurements	80% cut-off	0.03 (*a priori* volume)
			0.003 (background)
		60% cut-off	0.03 (*a priori* volume)
			0.003 (background)
		80% cut-off	0.06 (*a priori* volume)
			0.003 (background)
		60% cut-off	0.06 (*a priori* volume)
			0.003 (background)

Table 4

The estimated 3-D target location from multi-projection based fluorescence surface imaging studies for all experimental cases

Case#	True Target Location (cm)	Estimated Target Location (cm)
1	[1.5 2.5 2]	[1.5 2.7~3.0 2.5]
2	[2 2.5 2]	[1.7 2.7~2.9 2.3]
3	[2.5 2.5 2]	[2.4 2.6~3.1 1.7]
4	[2 2.5 2.5]	[2 2.2~2.5 2.3]
5	[2.5 2.5 2.5]	[2.5 2.1 2.1]

Table 5

Details of 3-D image reconstructions for a perfect uptake (1:0) phantom embedded with a single 0.45-cc fluorescing target at [1.5, 2.5, 2] cm.

		A priori Volume		Reconstructed [x y z] (cm)			Recovered Depth (cm) w.r.t Side A		Recovered Depth (cm) w.r.t Side B	
		Cut-off	Contrast	True	Recovered	Distance-off	True	Recovered	True	Recovered
Study I	(Side A)	N/A	N/A		[1.4 2.7 0.5]	1.52		0.5		N/A
	(Side B)	N/A	N/A		[0.5 2.4 1.9]	1.03		N/A		0.5
Study II	(Sides A+B)	N/A	N/A		[0.8 2.5 1.6]	0.78		1.6		0.8
Study III	(Sides A+B)	80%	20	[1.5 2.5 2]	[1.2 2.4 1.9]	0.30	2	1.9	1.5	1.2
		60%	20		[1.0 2.5 2.0]	0.48		2.0		1.0
		80%	10		[1.2 2.4 1.7]	0.45		1.7		1.2
		60%	10		[1.0 2.5 1.9]	0.49		1.9		1.0

Table 6

Details of 3-D image reconstructions for a perfect uptake (1:0) phantom embedded with a single 0.45-cc fluorescing target at [2, 2.5, 2] cm

							Recovered Depth (cm)			
		A priori Volume		Reconstructed [x y z] (cm)			w.r.t Side A		w.r.t Side B	
		Cut-off	Contrast	True	Recovered	Distance-off	True	Recovered	True	Recovered
Study I	(Side A)	N/A	N/A		[1.7 2.6 0.7]	1.36		0.7		N/A
	(Side B)	N/A	N/A		[0.7 3.1 2.3]	1.58		N/A		0.7
Study II	(Sides A+B)	N/A	N/A		[0.8 1.9 3.2]	1.82		3.2		0.8
Study III	(Sides A+B)	80%	20	[2 2.5 2]	[1.8 2.5 2.1]	0.22	2	2.1	2	1.8
		60%	20		[2.0 2.4 2.4]	0.4		2.4		2.0
		80%	10		[1.8 2.5 2.1]	0.22		2.1		1.8
		60%	10		[2.0 2.4 2.4]	0.4		2.4		1.8

Table 7

Details of 3-D image reconstructions for a perfect uptake (1:0) phantom embedded with a single 0.45-cc fluorescing target at [2.5, 2.5, 2] cm

							Recovered Depth (cm)			
		A priori Volume		Reconstructed [x y z] (cm)			w.r.t Side A		w.r.t Side B	
		Cut-off	Contrast	True	Recovered	Distance-off	True	Recovered	True	Recovered
Study I	(Side A)	N/A	N/A		[2.1 2.6 0.6]	1.42		0.6		N/A
	(Side B)	N/A	N/A		[0.9 2.9 2.0]	1.63		N/A		0.9
Study II	(Sides A+B)	N/A	N/A		[0.7 2.7 1.4]	1.89		1.4		0.7
Study III	(Sides A+B)	80%	20	[2.5 2.5 2]	[1.8 2.2 2.1]	0.70	2	2.1	2.5	1.8
		60%	20		[1.5 2.6 2.1]	1.02		2.1		1.5
		80%	10		[1.5 2.4 1.9]	0.98		1.9		1.5
		60%	10		[1.5 2.6 2.1]	1.02		2.1		1.5

Table 8

Details of 3-D image reconstructions for a perfect uptake (1:0) phantom embedded with a single 0.45-cc fluorescing target at [2, 2.5, 2.5] cm

		A priori Volume		Reconstructed [x y z] (cm)			Recovered Depth (cm) w.r.t Side A		Recovered Depth (cm) w.r.t Side B	
		Cut-off	Contrast	True	Recovered	Distance-off	True	Recovered	True	Recovered
Study I	(Side A)	N/A	N/A		[1.9 2.5 0.7]	1.83		0.7		N/A
	(Side B)	N/A	N/A		[1.1 2.5 2.5]	0.94		N/A		1.1
Study II	(Sides A+B)	N/A	N/A		[0.4 3.8 7.7]	5.57		7.7		0.4
Study III	(Sides A+B)	80%	20	[2 2.5 2.5]	[2.1 2.3 2.4]	0.22	2.5	2.4	2	2.1
		60%	20		[2.1 2.3 2.4]	0.23		2.4		2.1
		80%	10		[2.1 2.3 2.4]	0.22		2.4		2.1
		60%	10		[2.1 2.3 2.4]	0.23		2.4		2.1

Table 9

Details of 3-D image reconstructions for a perfect uptake (1:0) phantom embedded with a single 0.45-cc fluorescing target at [2.5, 2.5, 2.5] cm

		A priori Volume		Reconstructed [x y z] (cm)			Recovered Depth (cm) w.r.t Side A		Recovered Depth (cm) w.r.t Side B	
		Cut-off	Contrast	True	Recovered	Distance-off	True	Recovered	True	Recovered
Study I	(Side A)	N/A	N/A		[2.4 2.4 0.7]	1.84		0.7		N/A
	(Side B)	N/A	N/A		[0.4 1.9 2.2]	2.21		N/A		0.4
Study II	(Sides A+B)	N/A	N/A		[3.7 1.7 0.9]	2.18		0.9		3.7
Study III	(Sides A+B)	80%	20	[2.5 2.5 2.5]	[2.7 2.2 2.1]	0.56	2.5	2.1	2.5	2.7
		60%	20		[2.5 2.1 1.9]	0.76		1.9		2.5
		80%	10		[2.7 2.0 2.1]	0.56		2.1		2.7
		60%	10		[2.5 2.1 1.9]	0.74		1.9		2.5